Time-domain interferometry of electron weak localization through terahertz nonlinear response

Zi-Long Li [1,2,*] Xiao-Hui Li [1,2,*] and Yuan Wan [1,3,†]
[1] *Institute of Physics, Chinese Academy of Sciences, Beijing 100190, China*
[2] *University of Chinese Academy of Sciences, Beijing 100049, China*
[3] *Songshan Lake Materials Laboratory, Dongguan, Guangdong 523808, China*

(Received 12 May 2024; accepted 8 July 2024; published 2 August 2024)

We study theoretically the nonlinear optical response of disordered electrons in the regime of weak (anti)localization. Our analytical and numerical calculations reveal that in orthogonal/symplectic class systems, two consecutive, phase-coherent optical pulses generate an electric current echo that appears after the second pulse, and at a time equal to the pulse delay time. The current echo reflects the quantum interference between a self-intersecting electron path and its time-reversal partner, and, therefore, provides a time-domain interferometry of weak (anti)localization. Our results can be potentially tested on disordered metal films by using terahertz two-dimensional coherent spectroscopy or ultrafast transport measurements.

DOI: 10.1103/PhysRevResearch.6.033125

I. INTRODUCTION

Weak localization is the quintessential *quantum interference* phenomenon that features prominently in two-dimensional disordered conductors [1–4]. In such systems, the charge transport is determined by the sum over electron trajectories. Provided that the time-reversal symmetry is present and the spin-orbit coupling is weak, a pair of time-reversed, self-intersecting trajectories has equal quantum amplitude and, therefore, would interfere constructively [5]. Electron weak localization emerges from this constructive interference process in that the latter reduces the electrical conductivity from the Drude conductivity. In the opposite limit of strong spin-orbit coupling, the weak antilocalization occurs due to the destructive interference of the trajectory pairs, resulting in an excessive conductivity [6].

A powerful diagnostic for the electron weak localization is the magnetoresistance [1,7]. Applying a weak magnetic field perpendicular to the conductor film breaks the time-reversal symmetry in a controlled way. The time-reversed trajectory pair now picks up Aharonov-Bohm (AB) fluxes that are opposite in sign. The magnetic field suppresses the weak localization by partially destroying the phase coherence between the pair of trajectories. The suppression results in a characteristic magnetoresistance curve, from which a key physical quantity such as the electron phase coherence length can be extracted.

The magnetoresistance has been the canonical diagnostic for electron weak localization since the latter's discovery. Yet, other mechanisms for magnetoresistance, such as the Coulomb interaction [8,9], the superconducting fluctuation [10], as well as their interplay with weak localization, can significantly complicate the analysis of experimental data. Therefore, it is desirable to develop alternative diagnostics, which may allow for a cross examination of the data from independent experimental probes, thereby offering a more comprehensive view of the weak localization phenomenon.

In this work, we address the above problem by proposing that the terahertz nonlinear optical response is up for the task. It has long been recognized that the nonlinear optical response and the quantum interference are deeply linked [11–13]. We thus anticipate that the nonlinear optical response from disordered electrons may develop unique signatures tied to the weak localization. Meanwhile, the terahertz frequency window matches well with the timescale for electron weak localization, namely, the phase coherence time τ_ϕ, which is of the order of a few picoseconds at a temperature $\sim O(10)$ Kelvin [1,14].

Specifically, we analyze the nonlinear electric current generated by two consecutive, phase-coherent terahertz pulses, with polarization parallel to the conductor film [Fig. 1(a)]. The two pulses are separated by a delay time τ. For the sake of simplicity, we omit the electron-electron and electron-phonon interactions at the outset. Their impact on weak localization is subsumed in a phenomenological electron phase coherence time τ_ϕ added by hand. We focus on two prototypical symmetry classes of the disorder [15], i.e., the orthogonal class and the symplectic class, which describe a disordered metal in the limit of zero and strong spin-orbit coupling, respectively.

Our field theory analysis, as well as numerical simulations, reveal that the nonlinear current, measured as a function of time t_g *after the second pulse* (dubbed the gating time), exhibits a peak [Fig. 1(b)]. Crucially, the peak appears at the gating time $t_g = \tau$. As the pulse delay time τ increases, the

*These authors contribute equally to this work.
†Contact author: yuan.wan@iphy.ac.cn

Published by the American Physical Society under the terms of the Creative Commons Attribution 4.0 International license. Further distribution of this work must maintain attribution to the author(s) and the published article's title, journal citation, and DOI.

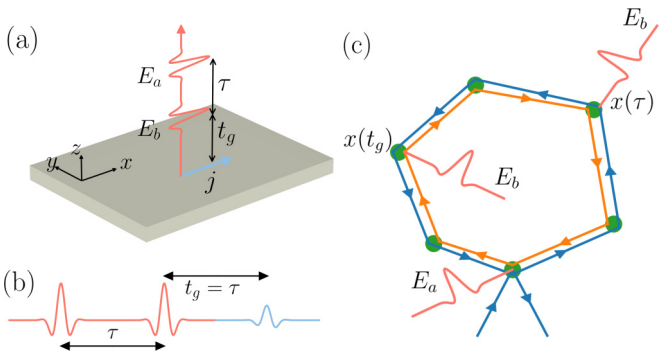

FIG. 1. (a) Two linearly polarized, phase-coherent terahertz pulses (E_a and E_b) with delay time τ generates a nonlinear electric current (j) in the disordered metal film. (b) j exhibits an echo at gating time $t_g = \tau$. (c) The current echo arises from the interference between a pair of time-reversed trajectories (blue and yellow). When $t_g \neq \tau$, the trajectory pair acquires different dynamical phases as the electrons are at different locations when E_b kicks in. The loss of phase coherence suppresses weak localization. The weak localization is reinstated when $t_g = \tau$, which produces the echo.

peak appears later and later. This *echo* behavior originates from the interference of time-reversed trajectory pairs, the very same process responsible for weak localization. Heuristically, the first pulse launches electron trajectories at time 0. Among them, those that self-intersect at $t_g + \tau$ contribute to the nonlinear current at the time of measurement. For each trajectory, there is a time-reversed trajectory that also contributes. When $t_g \neq \tau$, the electrons are at different positions when the second pulse kicks in. As a result, the time-reversed pair would pick up different dynamical phases, thereby suppressing the weak localization. However, when $t_g = \tau$, the weak localization reemerges due to the restoration of time-reversal symmetry. This revival of weak localization gives rise to the echo.

The current echo signal, which is also on the picosecond scale, can be potentially detected by the terahertz two-dimensional coherent spectroscopy [16,17]. In this kind of experiment, one uses two phase-coherent terahertz pulses to excite the metal film, and measures the terahertz electromagnetic field radiated by the nonlinear current. Alternatively, the nonlinear current may be generated and measured on chip by using the latest time-resolved transport measurement techniques [18,19].

The nonlinear optical response utilizes the delay time τ and the gating time t_g as knobs to control the coherence between the pair of time-reversed trajectories. Therefore, it works as a *time-domain* interferometry for electron weak localization, which complements the magnetoresistance measurement since the latter, employing the AB effect, can be viewed as a space-domain interferometry.

Similar to the magnetoresistance, the nonlinear optical response provides a means to probe electron phase decoherence in disordered conductors. Inelastic scatterings due to electron-electron and electron-phonon interactions result in the phase decoherence. Consequently, the current echo fades away exponentially when the pulse delay time τ increases. In particular, the echo must disappear when τ is much larger than the electron phase coherence time τ_ϕ as the interference is no longer viable. One may then extract τ_ϕ by carefully monitoring the echo decay.

The study of the nonlinear optical response of disordered electrons has a rich and dynamic history [20–22]. It is therefore necessary to put our work in an appropriate context. The current echo in the nonlinear optical response of an Anderson insulator, namely, the *strong* localization regime, was revealed in Ref. [23] by drawing analogy with an ensemble of molecules subject to an inhomogeneous environment. The echo mechanism in this case is quite different from the weak localization regime. It is most easily understood in one dimension, where the strong disorder effectively breaks up the conductor into disconnected segments. Each segment can be viewed as a molecule, whose energy spectrum is drawn from a distribution. The echo then arises from the dephasing and rephasing processes triggered by the pulses akin to the Hahn echo [24,25]. Apparently, this mechanism requires no time-reversal symmetry since it does not rely on the interference of time-reversed electron trajectory pairs.

Much closer to the spirit of this work is Ref. [26], where an echo spectroscopy for weak localization was first proposed in the context of cold atoms in optical lattices. It was shown that the breaking and restoration of the time-reversal symmetry by a time-dependent perturbation can lead to the echo phenomenon. Yet, Ref. [26] focuses on physical observables such as position correlation or momentum distribution, which are natural in cold-atom experiments [27], but challenging to access with solid-state experimental tools. A main message of the present work, therefore, is that the echo from the *electron* weak localization can be directly observed through an ultrafast nonlinear optical response.

The rest of the manuscript is organized as follows. In Sec. II, we describe the problem setup and the main results, and provide a quick, heuristic derivation of these results. We give a more rigorous derivation of the results based on the nonlinear σ model in Sec. III. In Sec. IV, we test our analytical predictions by numerical simulations. Finally, we discuss issues with experimental feasibility and a few important open questions in Sec. V.

II. MAIN RESULTS

In this section, we present the main results from our analytical calculations. We first present a general expression for the electric current response to an arbitrary electric field in Sec. II A. We then specialize to the case of two consecutive optical pulses, and analyze the resulted current echo in Sec. II B. Finally, in Sec. II C, we give a heuristic derivation of the results.

A. Nonlinear current response

We set the stage by first describing the setup used in this work [Fig. 1(a)]. It is sufficient for our purpose to consider a dirty metal film consisting of noninteracting electrons. The interaction effects on weak localization are absorbed into a phenomenological constant, i.e., the electron phase-coherence time τ_ϕ. We assume the following hierarchy of timescales: $\hbar/E_F \ll \tau_e \ll \tau_\phi$, where E_F is the Fermi energy and τ_e is the

elastic scattering time. Note that the timescale of the terahertz pulse is less or comparable with τ_ϕ, but much greater than τ_e. In this *diffusive metal* regime, we may focus on the universal behavior of the weak localization as described by the nonlinear σ model.

We set the metal film in the xOy plane. The film is infinite in both the x and y directions and has zero thickness in the z direction. The linearly polarized, terahertz pulses propagate in z with their polarization $\parallel x$. The electric field, measured on the film, is denoted by $E(t)$. This electric field generates a current, which is $\parallel x$ and uniform in the xOy plane. We denote the sheet current density by $j(t)$.

With this setup, the current density $j(t)$ is given by

$$j(t) = \sigma_{\rm D} E(t) - \eta \frac{G_0}{2\pi} \int_{-\infty}^{t} \frac{e^{-f(t,t') - \frac{t-t'}{\tau_\phi}}}{t-t'} E(t') dt'. \quad (1)$$

Here, $\sigma_{\rm D}$ is the Drude conductance. The second term describes the weak localization correction. The parameter η encodes the underlying symmetry class [6],

$$\eta = \begin{cases} 1 & \text{(orthogonal)} \\ -\frac{1}{2} & \text{(symplectic)}. \end{cases} \quad (2)$$

Here, η reflects the weak localization and antilocalization in the limit of zero and strong spin-orbit coupling, respectively.[1] $G_0 = 2e^2/h$ is the conductance quantum.

The coherence factor $f(t,t')$ captures the suppression of the weak localization by a dynamical electric field,

$$f(t,t') = \frac{De^2}{\hbar^2} \int_{t'}^{t} [A(s) + A(t+t'-s) - 2\overline{A}]^2 ds, \quad (3a)$$

where

$$\overline{A} = \frac{1}{t-t'} \int_{t'}^{t} A(s) ds. \quad (3b)$$

Here, A is the vector potential in the Coulomb gauge, namely, $E = -\partial A/\partial t$. $\overline{A}$ is the "moving average" of the vector potential over the time window (t', t). It is easy to check that f is gauge invariant in the sense that shifting $A(t)$ by an arbitrary constant does not change its value. D is the electron diffusion constant of the metal.

Equation (1) is applicable to arbitrary electric field $E(t)$ as long as its timescale is much larger than the elastic scattering time τ_e. In the limit of $E(t) \to 0$, $f \to 0$. Eq. (1) reduces to the familiar expression for the weak localization conductivity in the time domain. Said differently, the nonlinear response to a strong electric field is encoded in the coherence factor f. Furthermore, the effect of a dynamical electric field is nonperturbative in the sense that expanding $j(t)$ in powers of E yields secular terms. For instance, expanding $\exp(-f)$ to the first order in f results in a third-order nonlinear conductivity $\sigma^{(3)}$, whose magnitude grows with its time arguments, invalidating the naive perturbative expansion in E. Crucially, f depends on the temporal profile of A as well as its time reversal with respect to $(t+t')/2$. This structure is responsible for the echo phenomenon described in Sec. II B.

B. Current echo

We apply Eq. (1) to the case of two consecutive optical pulses. We illustrate the echo phenomenon by assuming that the optical pulses are sufficiently short so that they may be modeled as Dirac-δ functions,

$$E(t) = E_a \Delta \delta(t) + E_b \Delta \delta(t-\tau). \quad (4)$$

Here, $E_{a,b}$ and Δ are, respectively, the peak electric field strength and the pulse duration. The pulse A arrives at the film at time 0 and the pulse B at time τ. The vector potential is given by

$$A(t) = -E_a \Delta \Theta(t) - E_b \Delta \Theta(t-\tau). \quad (5)$$

Substituting the above into Eq. (1), we find the nonlinear current measured at the time $\tau + t_g$,

$$j_{ab}(\tau + t_g) = -\eta \frac{G_0}{2\pi} \frac{\Delta}{t_g + \tau} e^{-f(\tau+t_g,0) - \frac{\tau+t_g}{\tau_\phi}} E_a. \quad (6)$$

Here, j_{ab} is the nonlinear current that depends on both E_a and E_b, i.e., the cross effect of the two pulses. We have dropped terms that depend on E_a or E_b alone. The coherence factor is given by

$$f(\tau + t_g, 0) = \frac{2De^2 E_b^2 \Delta^2}{\hbar^2} \frac{|\tau - t_g|}{\tau + t_g} \min\{t_g, \tau\}. \quad (7)$$

Here, $\min\{t_g, \tau\}$ refers to the lesser of the two arguments.

Figure 2(c) shows j_{ab} calculated from Eq. (6) for the orthogonal class ($\eta = 1$). Results for the symplectic class ($\eta = -1/2$) can be obtained by multiplying the corresponding results by a factor of $-1/2$. We use representative material and pulse parameters: $D = 1$ cm^2/s, $\tau_\phi = 10$ ps, $E_a = E_b = 1$ kV/cm, and $\Delta = 1$ ps. For fixed pulse delay time τ, we observe a peak in the current response at $t_g = \tau$. This peak is the current echo signal described in Sec. I. Mathematically, this peak stems from the coherence factor: When $|t_g - \tau|$ is large, $f \gg 1$, which, in turn, suppresses j_{ab} exponentially. However, when $\tau = t_g$, $f = 0$, thereby exposing the contribution due to weak localization.

The maximum of j_{ab}, located at $t_g = \tau$, is given by

$$j_{ab}(2\tau) = -\eta \frac{G_0}{2\pi} \frac{\Delta}{2\tau} e^{-2\tau/\tau_\phi} E_a. \quad (8)$$

We see that the height of the peak traces the electron decoherence. As the pulse delay τ increases, the peak appears later and later; meanwhile, its magnitude decreases. The peak eventually vanishes when $\tau \gg \tau_\phi$. Thus, we may extract the coherence time τ_ϕ by carefully monitoring how the echo fades away with τ.

The width of the peak, W, can be tuned by the pulse parameters E_b and Δ, namely, $W \propto 1/(E_b\Delta)^2$. Specifically, a stronger pulse makes the peak sharper. Experimentally, one may choose appropriate E_b such that the width of the peak matches the time resolution of the instrument.

[1] We use a simplified model where the spin-orbit coupling manifests in the skewed impurity scattering that mixes electron spin [6]. Although this model cannot capture the rich spin-orbit coupling phenomenon in real materials, it is sufficient for analyzing the universal features of weak localization at low energy.

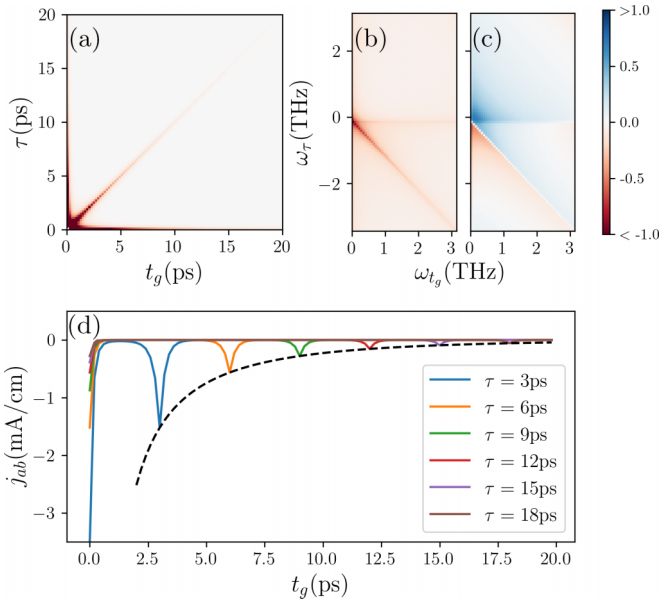

FIG. 2. (a) Nonlinear current density j_{ab} as a function of the pulse delay time τ and the gating time t_g for the orthogonal class ($\eta = 1$) and Dirac-δ pulses. [(b),(c)] The real and imaginary parts of the two-dimensional coherent spectrum, obtained by Fourier transforming the time-domain data shown in (a). Only the first and fourth quadrants are shown as the spectrum in the other half plane is related by complex conjugation. (d) t_g scan of the time-domain data for representative values of τ. Dashed line traces the peaks of the current echo. Note that the data in [(a)–(c)] are in arbitrary units, whereas (d) shows the original data without any rescaling.

The echo signal can be measured by using the terahertz two-dimensional coherent spectroscopy [16,17]. The experimental setup is identical to the one considered in this section. The spectroscopy detects the current echo through the latter's terahertz electromagnetic radiation. Scanning both t_g and τ produces a two-dimensional plot for the nonlinear signal [Fig. 2(a)]. The echo manifests itself as the diagonal feature extending up to τ_ϕ. The two-dimensional spectrum is then obtained by Fourier transforming the time-domain data [Figs. 2(b) and 2(c)]. The echo appears as a highly anisotropic peak in the fourth quadrant. The width of the peak in the antidiagonal direction is approximately proportional to $1/\tau_\phi$, whereas the width of the peak in the diagonal direction is controlled by $1/W$.

Having illustrated the current echo phenomenon, we now show that the phenomenon is robust with more realistic pulse profiles. To this end, we use single-cycle pulses: $E(t) = E_a e^{-\frac{t^2}{2\Delta^2}} \cos(\omega_0 t) + E_b e^{-\frac{(t-\tau)^2}{2\Delta^2}} \cos[\omega_0(t-\tau)]$. Figure 3 shows the nonlinear current j_{ab} obtained by numerical integration of Eq. (1). We set the central frequency $\omega_0 = 3$ THz. $E_a = E_b = 1$ kV/cm. $\Delta = 0.707$ ps. The material parameters are $D = 2$ cm^2/s and $1/\tau_\phi = 0$. The current echo peak is clearly visible, but the overall magnitude of the signal is weaker than that of the Dirac-δ pulses. This is due to the fact that the single-cycle pulse with the same value of E_a and Δ has less area under the pulse.

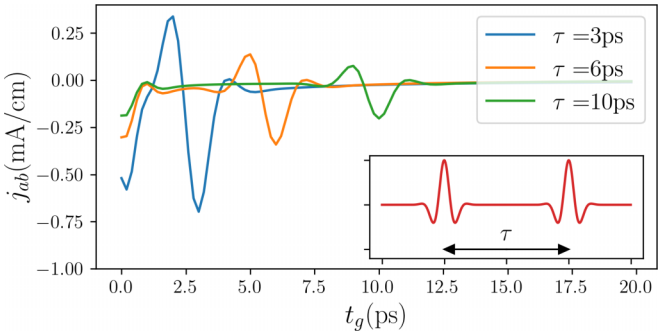

FIG. 3. Nonlinear current density j_{ab} as a function of gating time t_g (solid lines) induced by single-cycle pulses (inset) for representative values of pulse delay time τ.

C. Heuristic derivation

We derive Eq. (1) heuristically by adapting the semiclassical treatment of Ref. [2] to the problem at hand. We consider the orthogonal class ($\eta = 1$) for simplicity. To this end, we consider the probability density for the electron to start at time t' from some position and return to the same position at later time t, dubbed $W(t,t')$. $W(t,t')$ may be expressed as a double path integral,

$$W(t,t') = \int Dr' Dr e^{\frac{i}{\hbar}(S[r]-S[r'])}, \tag{9}$$

where r and r', respectively, correspond to the forward and backward time evolution. $r(t) = r(t') = 0$, and the same holds for r'. S is the action,

$$S[r] = \int_{t'}^{t} \left[\frac{m\dot{r}^2}{2} - V(r) + eA^\alpha(s)\dot{r}^\alpha(s)\right] ds, \tag{10}$$

where $V(r)$ represents the disorder potential. $A^a(s)$ is the time-dependent, spatially uniform vector potential due to the terahertz pulse. $\alpha = x, y$ labels the Cartesian components.

Due to the disorder potential, the paths r and r' are phase incoherent, except for two special cases. The first case is $r(s) = r'(s)$, i.e., the forward and backward paths are identical. They are always in phase because $S[r] = S[r']$. Responsible for the weak localization is the second case, $r(s) = r'(t + t' - s)$, i.e., the two trajectories are time-reversal partners. We have

$$\begin{aligned} i(S[r] - S[r']) &= ie \int_{t'}^{t} A^\alpha(s)[\dot{r}^\alpha(s) - \dot{r}'^\alpha(s)] ds \\ &= ie \int_{t'}^{t} [A^\alpha(s) + A^\alpha(t + t' - s)]\dot{r}^\alpha(s) ds. \end{aligned} \tag{11}$$

Therefore, they are almost in phase barring the dynamical vector potential. We may express its contribution to W as

$$\widetilde{W}(t,t') = \langle e^{i\frac{e}{\hbar}\int_{t'}^{t}[A^\alpha(s)+A^\alpha(t+t'-s)]\dot{r}^\alpha(s)ds} \rangle, \tag{12}$$

where the average is over closed paths r. $\widetilde{W}$ is a measure of weak localization correction to electron transport [2].

As the electron essentially undergoes random walk due to disorder potential scattering, we may well approximate r as Brownian motion. We discretize the time evolution into slices.

Over a time slice dt, the electron displacement is given by dr^α, where dr^α is a Gaussian random vector with variance $\langle dr^\alpha dr^\beta\rangle = 2Ddt\delta^{\alpha\beta}$, with D being the electron diffusion constant. We thus have

$$\widetilde{W}(t,t') = \left\langle \delta\left(\sum_s dr_s\right) e^{i\frac{e}{\hbar}\sum_s [A^\alpha(s)+A^\alpha(t+t'-s)]dr_s^\alpha}\right\rangle. \tag{13}$$

The average is now over dr_s^a. The Dirac-δ function enforces the constraint that r starts from and returns to the same location. It can be replaced by an integration over the Lagrange multiplier q^α,

$$\begin{aligned}\widetilde{W}(t,t') &= \left\langle \int \frac{d^2q}{(2\pi)^2} e^{i\sum_s\{q^\alpha+\frac{e}{\hbar}[A^\alpha(s)+A^\alpha(t+t'-s)]\}dr_s^\alpha}\right\rangle \\ &= \int \frac{d^2q}{(2\pi)^2} e^{-D\int_{t'}^t\{q^\alpha+\frac{e}{\hbar}[A^\alpha(s)+A^\alpha(t+t'-s)]\}^2 ds}.\end{aligned} \tag{14}$$

In the second line, we average over dr_s^α and then take the continuous limit $dt \to 0$. Integrating over q^α, we obtain

$$\widetilde{W}(t,t') = \frac{e^{-f(t,t')}}{4\pi D(t-t')}, \tag{15}$$

where f is the coherence factor given by Eq. (3). Up to a constant prefactor, $\widetilde{W}$ is essentially the same as the weak localization part of Eq. (1). The phase-coherent time τ_ϕ in Eq. (1) is added by hand.

This heuristic derivation shows that the coherence factor captures the suppression of the phase coherence between a pair of time-reversed electron trajectories by a time-dependent electric field. Specializing to the case considered in Sec. II B, we may compare the dynamical phases picked up by $r(s)$ and its time-reversal partner $r(\tau + t_g - s)$ [Fig. 1(b)] [26]. For the former path, the dynamical phase due to pulse B is given by $e\int A^\alpha(s)\dot{r}^\alpha(s)ds/\hbar \sim e\hbar\int r^\alpha(s)E^\alpha(s)ds/\hbar = ex(\tau)E_b/\hbar$. For the latter path, the phase is $ex(t_g)E_b/\hbar$. Therefore, the two paths accumulate different phases when $t_g \neq \tau$. However, when $t_g = \tau$, the two paths acquire the same dynamical phase. The loss and reinstatement of phase coherence leads to the suppression and resurgence of the weak localization, which, in turn, produces the current echo.

III. FIELD THEORY

In this section, we justify Eq. (1) by field theory [28]. Although it can be obtained by adapting the classic analysis of Ref. [29], the present treatment provides a rigorous and systematic derivation from the perspective of the effective action. As we shall see, Eq. (1) results from the one-loop approximation to the effective action, which, in principle, can be improved by going to high orders in the loop expansion. Our derivation is also partly pedagogical in that it serves to connect the field theory approach to more well-spread methods such as the quantum kinetic equation and Cooperon equations. We illustrate the procedure for the orthogonal class. Since the calculations for the symplectic class are largely in parallel, we refer the interested reader to Appendix A for a brief discussion of this class.

In the orthogonal class, it is sufficient to consider spinless electrons because spin-up and -down states are decoupled. The starting point is the nonlinear σ model defined by the action (we use $\hbar = e = 1$ in this section),

$$iS[Q] = \frac{\pi N_F}{2}\mathrm{Tr}\left(\check{\partial}_t\check{Q} - \frac{D}{4}\nabla_A^\alpha\check{Q}\nabla_A^\alpha\check{Q}\right), \tag{16}$$

where N_F is the density of states *per spin* at the Fermi level. Tr denotes the trace over all the matrix indices as well as integration over space.

$\check{Q}(r)$ is the $4N_t \times 4N_t$ matrix field in the time-reversal $\otimes$ Keldysh space, where N_t is the number of time slices. $\check{Q}$ is subject to the following constraints:

$$\check{Q}^2 = \check{I};\ \check{Q}^\dagger = \check{Q};\ \check{Y}\check{Q}\check{Y} = -\check{Q}^T;\ \check{Y} \equiv \begin{pmatrix} 0 & \hat{I} \\ -\hat{I} & 0\end{pmatrix}. \tag{17}$$

We use the convention that $\check{M}$ stands for a $4N_t \times 4N_t$ matrix in the time-reversal $\otimes$ Keldysh space, whereas $\hat{M}$ stands for a $2N_t \otimes 2N_t$ matrices in the Keldysh space. Furthermore, $\check{M}_{ts}$ refers to the 4×4 block of $\check{M}$ with designated time arguments t and s, whereas $\hat{M}_{ts}$ refers to the 2×2 block of $\hat{M}$.

$\check{\partial}_t$ is the time-derivative matrix written in the time-reversal space: $\check{\partial}_t \equiv \mathrm{diag}(\partial_t, \partial_t, -\partial_t, -\partial_t)$. $\nabla_A^\alpha\check{Q}$ is the gauge covariant derivative, $\nabla_A^\alpha\check{Q} \equiv \nabla^a\check{Q} - i[\check{A}^\alpha, \check{Q}]_-$, where $[\cdot,\cdot]_-$ stands for the matrix commutator. $\check{A}^\alpha \equiv \mathrm{diag}(A^\alpha, A^\alpha, -A^\alpha, -A^\alpha)$. We use the Coulomb gauge, $\nabla^\alpha A^\alpha = 0$.

We seek the effective action $\Gamma[\check{Q}_0]$, where $\check{Q}_0$ stands for the expectation value of $\check{Q}$. This strategy is motivated by the observation that the charge density is related to $\check{Q}_0$ through the following relation:

$$\rho(r,t) = \frac{\pi N_F N_s}{4}\mathrm{tr}[\check{\gamma}_q\check{Q}_{0,tt}(r)]. \tag{18}$$

Here, $N_s = 2$ is the number of spin species. $\check{\gamma}_q$ is the 4×4 charge density vertex: $\check{\gamma}_q = \mathrm{diag}(\hat{\tau}^1, \hat{\tau}^1)$, where $\hat{\tau}^1$ is the first Pauli matrix. As a result, the stationary point of the effective action, $\delta\Gamma[\check{Q}_0]/\delta\check{Q}_0 = 0$, encodes the charge transport equation. In what follows, we illustrate the procedure step by step.

A. Parametrizing the stationary point

We write the stationary point as

$$\check{Q}_0(r) = \check{R}(r)\check{\Lambda}\check{R}(r)^{-1}. \tag{19a}$$

$\check{\Lambda} \equiv \mathrm{diag}(I, -I, I, -I)$ is a constant matrix. $\check{R}(r)$ is a block diagonal matrix that parametrizes the stationary point,

$$\check{R}(r) = \mathrm{diag}[\hat{R}(r), \hat{R}(r)^{T,-1}], \tag{19b}$$

where the block $\hat{R}$, in turn, is given by

$$\hat{R}(r) = \begin{pmatrix} I & 0 \\ Z(r) & I\end{pmatrix}\begin{pmatrix} I & F(r) \\ 0 & -I\end{pmatrix}. \tag{19c}$$

$F(r)$ and $Z(r)$ are $N_t \times N_t$ matrix fields parametrizing the stationary point. F plays the role of distribution function, whereas Z describes the deviation of $\check{Q}_0$ from the causal form. When $Z = 0$, $\check{Q}_0$ is causal.

We bring in the fluctuations by writing

$$\check{Q}(r) = \check{R}(r)\exp\left[\frac{i}{2}\check{G}(r)\right]\check{\Lambda}\exp\left[-\frac{i}{2}\check{G}(r)\right]\check{R}(r). \tag{20}$$

$\check{G}$ generates soft fluctuations about the stationary point. The constraints on $\check{Q}$, as well as the requirement that $\check{G}$ must

induces nontrivial rotations on $\check{\Lambda}$, fixes $\check{G}$ to the following form:

$$\check{G}(r) = \begin{pmatrix} 0 & d(r) & 0 & c(r) \\ d(r)^\dagger & 0 & c(r)^T & 0 \\ 0 & c(r)^* & 0 & -d(r)^* \\ c(r)^\dagger & 0 & -d(r)^T & 0 \end{pmatrix}, \tag{21}$$

where $c(r)$ and $d(r)$ are $N_t \times N_t$ matrix fields corresponding to the diffusion and Cooperon, respectively.

B. Finding the stationary point

We substitute Eq. (20) and Eq. (21) into the action, and expand it to quadratic order in c and d:

$$iS[\check{Q}] = iS_0[F, Z] + iS_1[F, Z, c, d] + iS_2[F, Z, c, d]. \tag{22}$$

$iS_0[F, Z]$ is the value of the action at the stationary point. S_1 and S_2 are, respectively, linear and quadratic in c, d. At one loop, the effective action is given by [30]

$$i\Gamma[F, Z] = iS_0[F, Z] + \ln \int DcDd e^{iS_2[F,Z,c,d]}. \tag{23}$$

The first term is the tree level contribution; the second term is the one-loop correction.

In principle, we may find the stationary point by first computing $i\Gamma[F, Z]$ and then taking derivatives with respect to F, Z. Here, we take a shortcut. Setting $Z = 0$, the stationary point is causal and, consequently, all closed loops vanish. This fact implies $i\Gamma[F, 0] = 0$ for any F. We deduce that the stationary point is located at $(F, 0)$, with F being determined by

$$i\frac{\delta\Gamma}{\delta Z}\bigg|_{Z=0} = 0. \tag{24}$$

Substituting Eq. (23) into the above equation, we obtain

$$i\frac{\delta S_0}{\delta Z}\bigg|_{Z=0} + \left\langle i\frac{\delta S_2}{\delta Z}\bigg|_{Z=0} \right\rangle_{c,d} = 0. \tag{25}$$

The average is performed with respect to the fluctuations in c and d, which are governed by the action $S_2[F, Z = 0, c, d]$.

We now need the explicit expression for iS_0 and iS_2 to progress further. After some algebra, we find

$$iS_0 = 2\pi N_F \mathrm{Tr}\big\{[\partial_t, Z]_- F - D\big(\nabla_A^\alpha F\big)\big(\nabla_A^\alpha Z\big)\big\}, \tag{26a}$$

$$iS_2 = -\frac{\pi N_F}{2}\mathrm{Tr}\big\{c^\dagger[\partial_t, c]_+ + Dc^\dagger(-\nabla_A')^2 c - 2D\big(\nabla_A^\alpha Z\big)c\big(\nabla_A^\alpha F\big)^T c^*\big\} + \cdots. \tag{26b}$$

We have dropped from S_2 terms that do not contribute to the kinetic equation. $[\cdot,\cdot]_+$ denotes the anticommutator. $\nabla'^\alpha_A \equiv \nabla^\alpha - i[A, \cdot]_+$ is the covariant derivative for the Cooperon field.

Substituting the above expressions into the stationary point condition given by Eq. (25), we obtain the kinetic equation,

$$[\partial_t, F(r)]_- + \nabla_A^\alpha J_F^\alpha(r) = 0. \tag{27a}$$

J_F^α can be interpreted as a current associated to the distribution function,

$$\big[J_F^\alpha(r)\big]_{t_1t_1'} = -D\big[\nabla_A^\alpha F(r)\big]_{t_1t_1'} + \frac{D}{\pi N_F}\int dt_2 dt_2' \times \big[\nabla_A^\alpha F(r)\big]_{t_2t_2'} \mathcal{C}_{t_1t_2',t_2t_1'}(r, r). \tag{27b}$$

The first term comes from the classical action iS_0; the second arises from the correction due to the fluctuations in the Cooperon field, namely, $i\langle \delta S_2/\delta Z\rangle_{c,d}$. The Cooperon propagator is

$$\mathcal{C}_{t_1t_1',t_2t_2'}(r_1, r_2) \equiv \frac{\pi N_F}{2}\big\langle c_{t_1t_1'}(r_1)c^*_{t_2t_2'}(r_2)\big\rangle. \tag{28}$$

It obeys the Cooperon equation [29]

$$\Big\{\partial_{t_1} - \partial_{t_1'} + D[-i\nabla^\alpha - A^\alpha(r_1, t_1) - A^\alpha(r_1, t_1')]^2 + \frac{1}{\tau_\phi}\Big\}\mathcal{C}_{t_1t_1',t_2t_2'}(r_1, r_2) = \delta_{t_1t_2}\delta_{s_1s_2}\delta_{r_1r_2}. \tag{29}$$

Equation (29) can be read off from the kernel of the quadratic action iS_2. Here, we have added a mass term $1/\tau_\phi$ by hand to account for electron decoherence effects.

C. Charge transport equation

The next step is to extract a charge transport equation from the kinetic equation given by Eq. (27). It is convenient to perform a change of time variables to the central time $T = (t_1 + t_1')/2$ and the time difference $s = t_1 - t_1'$ [29]. The Cooperon propagator is diagonal in T,

$$\mathcal{C}^{TT'}_{ss'} \equiv \mathcal{C}_{T+\frac{s}{2},T-\frac{s}{2};T'+\frac{s'}{2},T'-\frac{s'}{2}} = \mathcal{C}^T_{ss'}\delta^{TT'}. \tag{30}$$

The superscripts (subscripts) correspond to the central times (time differences). The Cooperon equation now acquires a simplified form,

$$\Big\{2\partial_s + D\big[-i\nabla^\alpha - A_s^{\alpha,T}(r)\big]^2 + \frac{1}{\tau_\phi}\Big\}\mathcal{C}^T_{ss'} = \delta_{ss'}\delta_{rr'}. \tag{31}$$

The shorthand notation $A_s^{\alpha,T}(r) = A^\alpha(r, T + s/2) + A^\alpha(r, T - s/2)$. Meanwhile, the kinetic equation reads

$$\partial_T F_s^T + \big[\nabla_A^\alpha J_F^\alpha(r)\big]_s^T = 0, \tag{32a}$$

$$\big[J_F^\alpha(r)\big]_s^T = -D\big(\nabla_A^\alpha F\big)_s^T + \frac{2D}{\pi N_F}\int dT' \times \big[\nabla_A^\alpha F(r)\big]_s^{T'} \mathcal{C}^{\frac{T+T'}{2}}_{T-T'+s,T'-T+s}(r, r). \tag{32b}$$

To make contact with the charge density, we substitute Eq. (19) (with $Z = 0$) into Eq. (18),

$$\rho(r, T) = \pi N_F N_s F^T_{s=0}(r). \tag{33}$$

Therefore, the charge density is given by the $s = 0$ component of the distribution function F_s^T. We observe that s appears as a parameter in the kinetic equation. Setting $s = 0$ and massaging the equations a little, we obtain the charge conservation law,

$$\partial_t \rho + \nabla^\alpha j^\alpha = 0. \tag{34a}$$

The electric current j^a obeys a generalized Fick's law,

$$j^\alpha(r,t) = -\int D_{tt'}(r)(\nabla^\alpha \rho - N_F N_s E^\alpha)(r,t')dt'. \quad (34b)$$

The nonlocal diffusion constant is given by

$$D_{tt'}(r) = D\delta_{tt'} - \frac{2D}{\pi N_F}\mathcal{C}^{\frac{t+t'}{2}}_{t-t',t'-t}(r,r). \quad (34c)$$

Equation (34) is the key result of this section.

Finally, we apply Eq. (34) to the case considered in Sec. II. $\nabla^\alpha\rho = 0$ because the electric field E is spatially uniform. The electric current reads

$$j(t) = \sigma_D E(t) - \frac{2N_s D}{\pi}\int \mathcal{C}^{\frac{t+t'}{2}}_{t-t',t'-t}(r,r)E(t')dt'. \quad (35)$$

Here, $\sigma_D = N_F N_s D$ is the Drude conductance. Solving the Cooperon equation by a spatial Fourier transform, we find the equal-position Cooperon propagator,

$$\mathcal{C}^{\frac{t+t'}{2}}_{t-t',t'-t}(r,r) = \theta(t-t')\frac{e^{-(t-t')/\tau_\phi}}{8\pi D(t-t')}e^{-f(t,t')}, \quad (36)$$

where $f(t,t')$ is the coherence factor given by Eq. (3). Substituting the above into the expression for the current, we obtain Eq. (1) for the orthogonal class after restoring $\hbar$ and e.

IV. NUMERICAL TESTS

In this section, we test the analytic predictions from Sec. II by a direct numerical simulation. We describe our numerical methodology in Sec. IV A. The numerical results are presented in Sec. IV B. Throughout this section, we use the natural units $\hbar = e = 1$.

A. Model and method

We model the disordered electrons by a tight-binding model on an $L \times L$ square lattice subject to periodic boundary conditions,

$$H = -\sum_{\langle mn\rangle\sigma} R(m,n)_{\sigma\sigma'}c^\dagger_{m\sigma}c_{n\sigma'} + \sum_{n\sigma} h_n c^\dagger_{n\sigma}c_{n\sigma}. \quad (37)$$

Here, $c_{n\sigma}$ ($c^\dagger_{n\sigma}$) annihilates (creates) an electron with spin σ on site i. $\langle mn\rangle$ labels the *oriented* nearest-neighbor bonds on the square lattice. We rescale the unit of energy such that the hopping amplitude is 1. h_n describes the on-site disorder potential; it is drawn uniformly from $[-V, V]$.

$R(m,n) \equiv R(n,m)^\dagger$ is a 2×2 matrix in the spin space [31]. Its form depends on the symmetry class,

$$R(m,n) = e^{iA_{mn}(t)} \times \begin{cases} I & \text{(orthogonal)} \\ g \in \mathrm{SU}(2) & \text{(symplectic)}. \end{cases} \quad (38)$$

Here, g is a random SU(2) matrix uniformly drawn from the Haar measure. $A_{mn}(t) = A^\alpha(t)(r^\alpha_m - r^\alpha_n)$ is the time-dependent vector potential on the bond mn, through which the electromagnetic field pulse acts on the electrons.

The quantity of interest is the electric current density generated by the time-dependent electric field,

$$j^\alpha(t) = \int d\epsilon n_f(\epsilon)\mathrm{tr}[U(t)^\dagger J^\alpha(t)U(t)\delta(\epsilon - H_0)]. \quad (39)$$

Here, $n_f(\epsilon)$ is the Fermi-Dirac distribution function. $J^\alpha(t)$ and $U(t)$ are, respectively, the current density operator and the time evolution operator in the *one-electron* state space. H_0 is the initial Hamiltonian before the impact of the electric field.

We employ the kernel polynomial method to evaluate Eq. (39) [32]. To this end, we rescale the Hamiltonian such that its entire spectrum falls inside the interval $[-1, 1]$. Expanding the Dirac-δ function in Eq. (39) by Chebyshev polynomials, we obtain

$$j^\alpha(t) = \sum_{n=0}^{M} c_n g_n \mu_n(t)\int d\epsilon \frac{n_f(\epsilon)}{\pi\sqrt{1-\epsilon^2}}T_n(\epsilon). \quad (40)$$

Here, M is the maximal expansion order. $c_n = 1/(1+\delta_{n,0})$. g_n is a coefficient due to the Jackson kernel. $T_n(\epsilon)$ is the nth Chebyshev polynomial of the first kind. μ_n are the nth Chebyshev moments,

$$\begin{aligned}\mu_n(t) &= \mathrm{Tr}[U(t)^\dagger J^\alpha(t)U(t)T_n(H_0)] \\ &= \frac{1}{R}\sum_r \langle r|U(t)^\dagger J^\alpha(t)U(t)T_n(H_0)|r\rangle. \end{aligned} \quad (41)$$

In the second line, we have replaced the trace by an average over random vectors $|r\rangle$, whose components are independently drawn from complex Gaussian distribution with variance 1. R is the number of random vectors used. The state $|r'\rangle = T_n(H)|r\rangle$ can be efficiently computed using the recursion relation. Meanwhile, we compute the unitary evolution of the states $U(t)|r\rangle$ and $U(t)|r'\rangle$ by using another Chebyshev expansion,

$$e^{-iH(t)\epsilon}|\psi\rangle = \sum_{n=0}^{M'}(-i)^n c_n J_n(\epsilon)T_n[H(t)]|\psi\rangle. \quad (42)$$

Here, $|\psi\rangle$ is a state vector. c_n is the same as in Eq. (40). $J_n(t)$ is the Bessel function of the first kind. ϵ is a small time interval. The above expansion rapidly converges when ϵ is small. The action of $T_n[H(t)]$ on $|\psi\rangle$, again, can be efficiently computed by using the recursion relation.

In practice, we use Dirac-δ pulses with $E_A\Delta = E_B\Delta = 1$ for simplicity. The electric field is polarized along the x direction. The strength of the on-site disorder potential is $V = 2$ in the orthogonal class, whereas it is $V = 1$ in the symplectic class. The system size $L = 1000$. As the Hilbert space dimension is 2×10^6, $R = 1$ is sufficient for computing the trace. We use $M = 50$ moments for computing the current density and $M' = 10$ for time evolution with $\epsilon = 1$. We average over 500 disorder samples to obtain good statistics for $j^x(t)$.

B. Numerical results

Figure 4 shows the numerically computed electric current generated by two consecutive Dirac-δ pulses. We set the temperature to 0 and the chemical potential E_F to the representative value -0.6. As the echo signal is independent of the polarization of the B pulse, we symmetrize our data with respect to E_b and $-E_b$ to remove undesired nonlinear responses. The current echo is clearly seen as the diagonal feature in the two-dimensional plot of the current as a function of the pulse delay time τ and the gating time t_g [Fig. 4(a)], in qualitative agreement with the analytical results shown

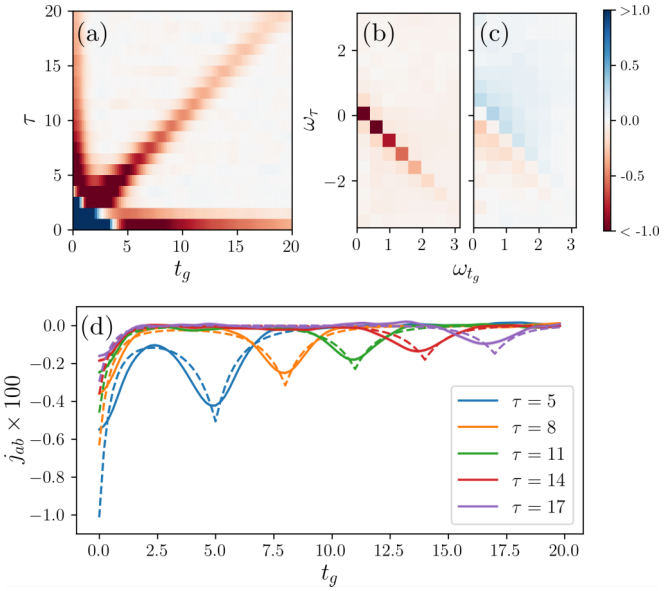

FIG. 4. (a) Numerically computed current density $j^x(t)$ as a function of the pulse delay time τ and the gating time t_g in the orthogonal class. The stronger linear response at short times is color saturated in order to reveal the current echo. [(b),(c)] The real and imaginary parts of two-dimensional Fourier transform of the data in (a). (d) t_g scan of the data in (a). The solid and dashed lines show, respectively, the numerical data and the analytical results given in Eq. (6). The shaded area denotes the error bar.

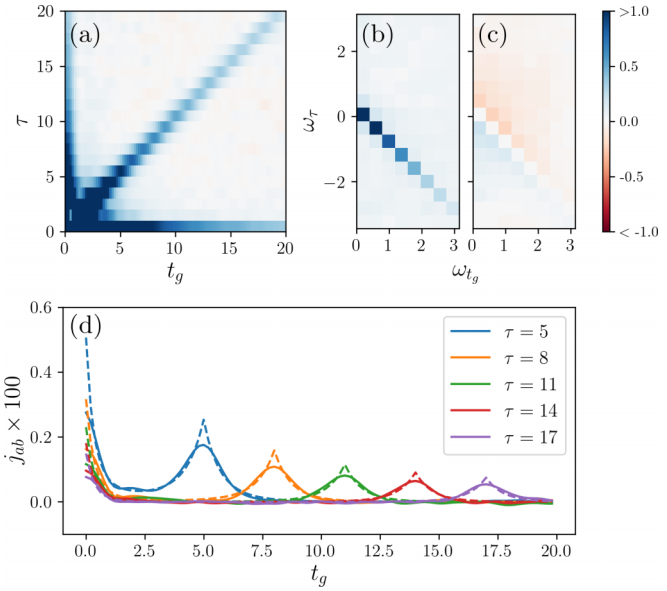

FIG. 5. Similar to Fig. 4, but for the symplectic class.

in Fig. 2. The two-dimensional spectrum also resembles its analytic counterpart [Figs. 4(b) and 4(c)].

Figure 4(d) shows a quantitative comparison between the numerical data (solid lines) and the analytic predictions (dashed lines). To this end, we fit Eq. (6) to the numerical data by adjusting the electron diffusion constant D, which is the only free parameter. We find $D \approx 1.04$ results in a good fit. We note that Eq. (6) predicts a cusp in the current echo peak, which is rounded off in the numerical data. This difference is likely due to the details of the electronic structure that are not captured by the field theory.

We find the same good agreement between the numerical data and the analytic predictions in the symplectic class (Fig. 5). Here, we set the temperature to 0 and the chemical potential $E_F = -0.57$. Compared with the orthogonal class, the echo in the symplectic class reduces by half in its magnitude and changes the sign. A fit of the analytic result given by Eq. (6) to the numerical data indicates that the diffusion constant $D \approx 1.37$.

We further corroborate our analytic results by investigating the behavior of the echo in the presence of an external magnetic field perpendicular to the film. We expect that the magnetic field suppresses the echo as it breaks the time-reversal symmetry. In the presence of the magnetic field B, the nonlinear current reads

$$j_{ab}(B, \tau + t_g) = \phi[2BD(\tau + t_g)]\, j_{ab}(0, \tau + t_g), \qquad (43)$$

where $\phi(x) \equiv x/\sinh(x)$. $j_{ab}(0, \tau + t_g)$ is the nonlinear current in the absence of the magnetic field given by Eq. (6). Note that Eq. (43) omits the magnetic field's Zeeman coupling to the electron spin as its impact on the weak localization is negligible compared with the orbital effect. We derive Eq. (43) by solving the Cooperon equation in the presence of magnetic field, and plugging the resulting Cooperon propagator in Eq. (34). The details of the calculation are provided in Appendix B.

Equation (43) indicates that the magnetic field results in the suppression of the nonlinear current response. The mechanism is the same as that of the magnetoresistance, namely, the time-reversed electron trajectory pairs pick up opposite AB phases. Figure 6 shows the current echo as a function of the magnetic field, measured in units of the magnetic flux per plaquette, for fixed pulse delay time τ. The model parameters are the same as in those for Fig. 4 (orthogonal class) and Fig. 5 (symplectic class). We see that the echo diminishes as the magnetic field increases for both symmetry classes. Furthermore, we find good agreement between the numerical data (solid lines) and analytic results (dashed lines) with the same fitting parameter, namely, $D = 1.04$ for the orthogonal class and $D = 1.37$ for the symplectic class.

V. DISCUSSION

In summary, we have analyzed the nonlinear optical response of a disordered metal in the weak localization regime. Our main finding is that two consecutive optical pulses, preferably in the terahertz range, can trigger a current echo response. This echo reflects the quantum interference between a pair of time-reversed electron trajectories, the same process that produces the weak localization. In particular, one may measure the electron coherence time by carefully monitoring the gradual decay of the echo signal as a function of the pulse delay.

This current echo can be detected by terahertz two-dimensional coherent spectroscopy [16,17] or ultrafast transport measurement [18,19], thereby offering an experimental diagnostic for electron weak localization complementary to

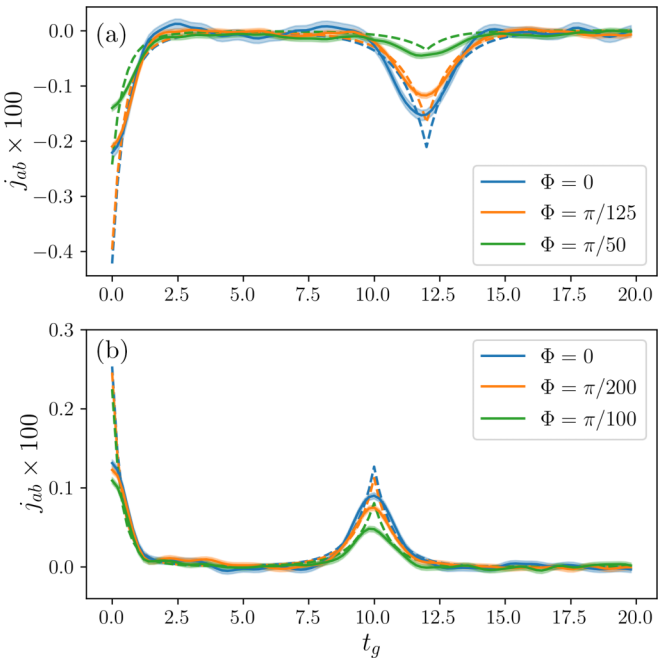

FIG. 6. The current echo in the presence of a perpendicular magnetic field. (a) The orthogonal class. The solid line represents the numerical data for three representative magnetic field strengths, measured in units of flux per plaquette Φ. The dashed line denotes the analytic result from Eq. (43). The shaded area marks the error bar. (b) Similar to (a), but for the symplectic model.

the magnetoresistance measurement. For a single layer of disordered metal, the current echo signal is of the order of $j \sim 1$ mA/cm with an excitation pulse $E_a = 1$ kV/cm (Fig. 2). The electric field strength of the terahertz radiation is of the order of $E = Z_0 j/2 \sim 0.2$ V/cm, which is weak but should be within the reach of available terahertz technology. We expect that stacking multiple layers would enhance the signal strength.

Our calculation focuses on the two opposite limits, namely, the weak (anti)localization in the limit of zero (strong) spin-orbit coupling (SOC). One may naturally ask what happens when the strength of the SOC does not fall into either of the two limits. In the presence of SOC, the Cooperon comes in two species, i.e., the spin singlet and the spin triplet. The singlet Cooperon is always gapless. By contrast, the triplet Cooperon acquires a gap that scales with the strength of SOC. In the limit of strong SOC, the triplet Cooperon is irrelevant to the electron dynamics. The singlet Cooperon alone is responsible for the weak antilocalization. However, with moderate SOC, the triplet Cooperon has a finite but small gap. In this case, we expect a crossover from the orthogonal class to the symplectic class, or weak localization to weak antilocalization as the relevant energy scale decreases. Specific to the echo phenomenon considered in the present work, we expect an interesting sign change in the echo signal as the pulse delay time τ exceeds the timescale set by the strength of SOC.

On the theory front, our work leaves a couple of interesting open questions. In deriving our results, we have made the simplifying assumption that the electrons are noninteracting. It is well known that the Coulomb interaction can lead to an anomalous correction to the linear conductivity; this correction has a functional dependence on the external magnetic field and frequency similar to the weak localization [8]. These two contributions must be carefully unravelled in the magnetoresistance measurement. Although we expect that the echo is robust against the Coulomb interaction, the latter might have a nontrivial impact on the nonlinear optical response. The approach presented in Sec. III will prove useful in treating this problem.

Another interesting open problem is the fate of the current echo as the system crosses over from the weak localization to the strong localization. As discussed in Sec. I, an echo also exists in the strong localization regime, albeit due to a very different mechanism. It is likely that as the system enters the strong localization regime, the mechanism discussed in this work gradually subsides as the second mechanism sets in. Exactly in which manner this unfolds is unclear at the moment.

In a broader context, our work attests to the profound connection between the nonlinear response and quantum interference, which we believe produces rich physics that calls for further exploration.

ACKNOWLEDGMENTS

We thank Tao Dong, Chushun Tian, and Yongqing Li for discussions, and Ulrich Höfer for bringing Ref. [23] to our attention. This work is supported by the National Natural Science Foundation of China (Grants No. 12250008 and No. 12188101), by the National Key R&D Program of China (Grant No. 2022YFA1403800), and by the Chinese Academy of Sciences through the Strategic Priority Research Program (Grant No. XDB33020300) and the Project for Young Scientists in Basic Research (Grant No. YSBR-059).

APPENDIX A: SYMPLECTIC CLASS

The derivation of the charge transport equation in the symplectic symmetry class is in the same vein as the orthogonal class. We therefore focus on the differences between the two classes. In the symplectic case, the spin-up and spin-down electrons are mixed by the spin-orbit coupling. The action of the corresponding nonlinear σ model reads

$$iS[Q] = \pi N_F \mathrm{Tr}\left(\check{\partial}_t \check{Q} - \frac{D}{4}\nabla_A^\alpha \check{Q} \nabla_A^\alpha \check{Q}\right). \tag{A1}$$

Compared with the action for the orthogonal class, there is an extra factor of 2 in front of the action, which reflects the fact that the spin-up and -down electrons both enter the action. The matrix field $\check{Q}$ is subject to a set of constraints,

$$\check{Q}^2 = \check{I};\ \check{Q}^\dagger = \check{Q};\ \check{X}\check{Q}\check{X} = \check{Q}^*;\ \check{X} \equiv \begin{pmatrix} 0 & \hat{I} \\ \hat{I} & 0 \end{pmatrix}. \tag{A2}$$

We see that the third constraint is different from the orthogonal class.

As with the orthogonal class, we parametrize the stationary point and the fluctuations about it as

$$\check{Q}(r) = \check{R}(r) \exp\left(i\frac{\check{G}(r)}{2}\right) \check{\Lambda} \exp\left(-i\frac{\check{G}(r)}{2}\right) \check{R}^{-1}(r). \tag{A3}$$

Here, the definitions of $\check{R}$ and $\check{\Lambda}$ are the same as the orthogonal class. In particular, $\check{R}$ parametrizes the stationary point through the matrix fields F and Z. However, the matrix field $\check{G}$, which describes fluctuations about the stationary point, acquires a different form due to the different constraint mentioned above,

$$\check{G}(r) = \begin{pmatrix} 0 & d(r) & 0 & c(r) \\ d^\dagger(r) & 0 & -c^T(r) & 0 \\ 0 & -c^*(r) & 0 & -d^*(r) \\ c^\dagger(r) & 0 & -d^T(r) & 0 \end{pmatrix}. \tag{A4}$$

Exponentiating $\check{G}$ produces the symmetric space $O(4N_t)/[O(2N_t)\otimes O(2N_t)]$. By contrast, exponentiating the $\check{G}$ in the orthogonal class yields the symmetric space $Sp(2N_t)/[Sp(N_t)\otimes Sp(N_t)]$.

Expanding the action up to quadratic order in c, d, we obtain

$$iS_0 = 4\pi N_F \mathrm{Tr}\big\{[\partial_t, Z]F - D\big(\nabla_A^\alpha F\big)\big(\nabla_A^\alpha Z\big)\big\} \tag{A5a}$$

and

$$\begin{aligned} iS_2 = &-\pi N_F \mathrm{Tr}\big\{c^\dagger[\partial_t, c]_+ + Dc^\dagger(-\nabla_A')^2 c \\ &+ 2D\big(\nabla_A^\alpha Z\big)c\big(\nabla_A^\alpha F\big)^T c^*\big\} + \cdots . \end{aligned} \tag{A5b}$$

We suppress terms in S_2 that do not contribute to the kinetic equation. Both expressions gain an extra factor of 2 compared to the corresponding expressions in the orthogonal class. More importantly, the sign in front of the $\nabla_A^\alpha Z(\nabla_A^\alpha F)^T$ term has a plus sign instead of the minus sign. This sign difference is responsible for the weak antilocalization effect in the symplectic class.

The kinetic equation and the charge transport equation can now be derived in the same vein. We find a slightly different diffusion constant,

$$D_{tt'}(r) = D\delta_{tt'} + \frac{D}{\pi N_F}\mathcal{C}^{\frac{t+t'}{2}}_{t-t',t'-t}(r, r). \tag{A6}$$

Here, the propagator $\mathcal{C}$ obeys the same Cooperon equation. We see that the Cooperon correction to the diffusion constant has an extra factor of $\eta = -1/2$ compared to the orthogonal class, which results in the $\eta = -1/2$ factor in the expression for the nonlinear current.

APPENDIX B: NONLINEAR CURRENT RESPONSE IN A PERPENDICULAR MAGNETIC FIELD

In this section, we compute the nonlinear current response in the presence of a static magnetic field perpendicular to the film. In the main text, we have shown that the sheet current density induced by a dynamical electric field reads

$$j(t) = \sigma_D E(t) - 4\eta G_0 D \int \mathcal{C}^{\frac{t+t'}{2}}_{t-t',t'-t}(r, r)E(t')dt'. \tag{B1}$$

Here, σ_D is the Drude conductance. $G_0 = 2e^2/\hbar$ is the conductance quantum. $\eta = 1$ $(-1/2)$ in the orthogonal (symplectic) class. Crucially, the weak localization is encoded in the Cooperon propagator $\mathcal{C}$, which is governed by the Cooperon equation,

$$\left\{2\partial_s + D\big[-i\nabla^\alpha - eA_s^{\alpha,T}(r)\big]^2 + \frac{1}{\tau_\phi}\right\}\mathcal{C}^T_{ss'}(r, r') = \delta_{ss'}\delta^2(r - r'). \tag{B2}$$

Here, we have used the shorthand notation,

$$A_s^{\alpha,T}(r) = A^\alpha\Big(r, T + \frac{s}{2}\Big) + A^\alpha\Big(r, T - \frac{s}{2}\Big). \tag{B3}$$

A^α is the vector potential in the Coulomb gauge, $\nabla^\alpha A^\alpha = 0$.

For the specific case considered here, we write the vector potential as

$$A^\alpha(r, t) = A_1^\alpha(t) + A_2^\alpha(r). \tag{B4}$$

Here, A_1^α describes a spatially uniform, linearly polarized electromagnetic field pulse,

$$E^\alpha(t) = -\frac{\partial A_1^\alpha}{\partial t}. \tag{B5}$$

A_2^α describes the static magnetic field perpendicular to the film,

$$A_2^x(x) = -\frac{B}{2}y, \quad A_2^y(x) = \frac{B}{2}x. \tag{B6}$$

We now need to solve the Cooperon equation for the specific choice of A considered above. The Cooperon equation has the form of the imaginary-time Schrödinger equation with the Hamiltonian,

$$\hat{H}(s) = D\big[-i\nabla^a - eA_{1,s}^{\alpha,T} - eA_2^\alpha(r)\big]^2 + \frac{1}{\tau_\phi}. \tag{B7}$$

Note that T is merely a parameter. As the Hamiltonian at different times s commutes, the Cooperon propagator admits the following formal solution:

$$\mathcal{C}^T_{ss'}(r, r') = \tfrac{1}{2}\Theta(s - s')e^{-\frac{s-s'}{2\tau_\phi}}\langle r|e^{-\frac{D}{2}\int_{s'}^{s}[-i\nabla^\alpha - eA_2^\alpha(r) - eA_{1,u}^{\alpha,T}]^2 du}|r'\rangle. \tag{B8}$$

We simplify the imaginary-time evolution operator by expanding the bracket in the Hamiltonian,

$$\begin{aligned} \int_{s'}^{s}\big[-i\nabla^\alpha - eA_2^a(r) - eA_{1,u}^{\alpha,T}\big]^2 du &= \int_{s'}^{s}\big[-i\nabla^\alpha - eA_2^\alpha(r) - eA_{1,u}^{\alpha,T} + e\overline{A}_1^\alpha - e\overline{A}_1^\alpha\big]^2 du \\ &= \big[-i\nabla^\alpha - eA_2^\alpha(r) - e\overline{A}_1^\alpha\big]^2(s - s') + e^2\int_{s'}^{s}\big(A_{1,u}^{\alpha,T} - \overline{A}_1^\alpha\big)^2 du. \end{aligned} \tag{B9}$$

Here, $\overline{A}_1^\alpha$ is the temporal average of A_1^α,

$$\overline{A}_1^\alpha = \frac{1}{s - s'}\int_{s'}^{s} A_{1,u}^{\alpha,T}\, du. \tag{B10}$$

Substituting the above back to Eq. (B8), we obtain

$$\begin{aligned}\mathcal{C}^T_{ss'}(r,r') &= \frac{1}{2}\Theta(s-s')e^{-\frac{e^2D}{2}\int_{s'}^{s}(A^{\alpha,T}_{1,u}-\overline{A}^{\alpha}_1)^2du}e^{-\frac{s-s'}{2\tau_\phi}}\langle r|e^{-\frac{D}{2}[-i\nabla^\alpha-eA^\alpha_2(r)-e\overline{A}^\alpha_1]^2(s-s')}|r'\rangle \\ &= \frac{1}{2}\Theta(s-s')e^{-\frac{e^2D}{2}\int_{s'}^{s}(A^{\alpha,T}_{1,u}-\overline{A}^{\alpha}_1)^2du}e^{-\frac{s-s'}{2\tau_\phi}}e^{ie\overline{A}_1\cdot(r-r')}\langle r|e^{-\frac{D}{2}[-i\nabla^\alpha-eA^\alpha_2(r)]^2(s-s')}|r'\rangle. \end{aligned} \tag{B11}$$

In the second line, we have performed a gauge transformation to remove the constant vector potential $\overline{A}^a_1$ in the Hamiltonian.

To proceed further, we insert the resolution of identity,

$$\mathcal{C}^T_{ss'}(r,r') = \frac{1}{2}\Theta(s-s')e^{-\frac{e^2D}{2}\int_{s'}^{s}(A^{\alpha,T}_{1,u}-\overline{A}^{\alpha}_1)^2du}e^{-\frac{s-s'}{2\tau_\phi}}e^{ie\overline{A}_1\cdot(r-r')}\sum_\lambda \psi_\lambda(r)\psi^*_\lambda(r')e^{-D\lambda(s-s')}. \tag{B12}$$

Here, ψ_λ is the solution for the Landau level problem,

$$\tfrac{1}{2}\big[-i\nabla^\alpha - eA^\alpha_1(r)\big]^2\psi_\lambda(x) = \lambda\psi_\lambda(r). \tag{B13}$$

Compared with the standard Landau level problem, the electron mass is 1 and the magnetic field strength is $2B$. Therefore, the eigenvalues are given by

$$\lambda_{n,m} = \big(n+\tfrac{1}{2}\big)2B. \tag{B14}$$

The eigenstates are given by

$$\psi_{n,m}(z) = \frac{1}{2\pi l_B^2}\frac{1}{\sqrt{n!(n+m)!}}\left(l_B\frac{\partial}{\partial z}-\frac{z^*}{4l_B}\right)^n\left(\frac{z}{l_B}\right)^{n+m}e^{-\frac{|z|^2}{4l_B^2}}. \tag{B15}$$

The magnetic length $l_B = 1/\sqrt{2B}$. $z = x+iy$.

We thus have obtained the general expression for the Cooperon propagator. Now, what enters the expression for the electric current is the equal-space propagator. Owing to the translation invariance of the problem, we may set $r = r'$ to the spatial origin. We note that $\psi_{n,m}(0) = 0$ when $m > 0$. Therefore, the summation is restricted to the subset with $m = 0$:

$$\mathcal{C}^T_{ss'}(r,r) = \frac{1}{2}\Theta(s-s')e^{-\frac{e^2D}{2}\int_{s'}^{s}(A^{\alpha,T}_{1,u}-\overline{A}^{\alpha}_1)^2du}e^{-\frac{s-s'}{2\tau_\phi}}\sum_n \psi_{n,0}(0)\psi^*_{n,0}(0)e^{-2DB(n+\frac{1}{2})(s-s')}. \tag{B16}$$

We now need to evaluate $\psi_{n,0}(0)$,

$$\psi_{n,0}(0) = \frac{1}{n!}\frac{1}{2\pi l_B^2}\left(\frac{\partial}{\partial z}\right)^n(z)^n e^{-\frac{|z|^2}{4l_B^2}}\bigg|_{z=0} = \frac{1}{n!}\frac{1}{2\pi l_B^2}\left[\left(\frac{\partial}{\partial z}\right)^n(z)^n\right]e^{-\frac{|z|^2}{4l_B^2}}\bigg|_{z=0} = \frac{n!}{n!}\frac{1}{2\pi l_B^2} = \frac{B}{\pi}. \tag{B17}$$

Substituting the above result back, we obtain

$$\begin{aligned}\mathcal{C}^T_{ss'}(r,r) &= \frac{1}{2}\Theta(s-s')e^{-\frac{e^2D}{2}\int_{s'}^{s}(A^{\alpha,T}_{1,u}-\overline{A}^{\alpha}_1)^2du}e^{-\frac{s-s'}{2\tau_\phi}}\frac{B}{\pi}\sum_n e^{-2DB(n+\frac{1}{2})(s-s')} \\ &= \Theta(s-s')e^{-\frac{e^2D}{2}\int_{s'}^{s}(A^{\alpha,T}_{1,u}-\overline{A}^{\alpha}_1)^2du}e^{-\frac{s-s'}{2\tau_\phi}}\frac{B}{4\pi\sinh[DB(s-s')]}. \end{aligned} \tag{B18}$$

Setting $T = (t+t')/2$, $s = t-t'$, and $s' = t'-t$, the above expression becomes

$$\mathcal{C}^{\frac{t+t'}{2}}_{t-t',t'-t}(x,x) = \Theta(t-t')e^{-f(t,t')}e^{-\frac{t-t'}{\tau_\phi}}\frac{B}{4\pi\sinh[2DB(t-t')]}. \tag{B19}$$

Here, $f(t,t')$ is the coherent factor defined in the main text,

$$\begin{aligned}f(t,t') &= \frac{e^2D}{2}\int_{t'-t}^{t-t'}\left[A^\alpha_1\left(\frac{t+t'+u}{2}\right)+A^\alpha_1\left(\frac{t+t'-u}{2}\right)-\overline{A}^\alpha_1\right]du \\ &= e^2D\int_{t'}^{t}\left[A^\alpha_1(u)+A^\alpha_1(t+t'-u)-\frac{2}{t-t'}\int_{t'}^{t}A^\alpha(u')du'\right]. \end{aligned} \tag{B20}$$

Plugging the above result into the expression for the current, we find

$$j(t) = \sigma_D E(t) - \eta\frac{G_0}{2\pi}\int_{-\infty}^{t}\phi[2DB(t-t')]\frac{e^{-f(t,t')-\frac{t-t'}{\tau_\phi}}}{t-t'}E(t')dt', \tag{B21}$$

where the function $\phi(x)$ encodes the impact of the magnetic field,

$$\phi(x) = \frac{x}{\sinh(x)}. \tag{B22}$$

Specializing to the case of two Dirac-δ pulses, we arrive at

$$j_{ab}(B, \tau + t_g) = \phi[2DB(\tau + t_g)] j_{ab}(0, \tau + t_g), \tag{B23}$$

which is the result given in the main text.

[1] G. Bergmann, Weak localization in thin films: A time-of-flight experiment with conduction electrons, Phys. Rep. **107**, 1 (1984).

[2] S. Chakravarty and A. Schmid, Weak localization: The quasiclassical theory of electrons in a random potential, Phys. Rep. **140**, 193 (1986).

[3] P. W. Anderson, E. Abrahams, and T. V. Ramakrishnan, Possible explanation of nonlinear conductivity in thin-film metal wires, Phys. Rev. Lett. **43**, 718 (1979).

[4] L. P. Gor'kov, A. I. Larkin, and D. E. Khmel'nitskiĭ, Particle conductivity in a two-dimensional random potential, Pis'ma Zh. Eksp. Teor, Fiz. **30**, 248 (1979) L. P. Gor'kov, A. I. Larkin, and D. E. Khmel'nitski, [JETP Lett. **30**, 228 (1979)].

[5] A. I. Larkin and D. E. Khmel'nitskiĭ, Anderson localization and anomalous magnetoresistance at low temperatures, Sov. Phys. Usp. **25**, 185 (1982).

[6] S. Hikami, A. I. Larkin, and Y. Nagaoka, Spin-orbit interaction and magnetoresistance in the two dimensional random system, Prog. Theor. Phys. **63**, 707 (1980).

[7] B. L. Altshuler, D. Khmel'nitzkii, A. I. Larkin, and P. A. Lee, Magnetoresistance and Hall effect in a disordered two-dimensional electron gas, Phys. Rev. B **22**, 5142 (1980).

[8] B. Altshuler and A. Aronov, Chapter 1 - Electron-electron interaction in disordered conductors, in *Electron–Electron Interactions in Disordered Systems*, Modern Problems in Condensed Matter Sciences, Vol. 10, edited by A. Eros and M. Pollak (Elsevier, Amsterdam, 1985), pp. 1–153.

[9] H. Fukuyama, Chapter 2 - Interaction effects in the weakly localized regime of two- and three-dimensional disordered systems, in *Electron-Electron Interactions in Disordered Systems*, Modern Problems in Condensed Matter Sciences, Vol. 10, edited by A. Efros and M. Pollak (Elsevier, Amsterdam, 1985), pp. 155–230.

[10] A. Larkin and A. Varlamov, *Theory of Fluctuations in Superconductors* (Oxford University Press, Oxford, 2005).

[11] S. Mukamel, *Principles of Nonlinear Optical Spectroscopy*, rev. ed. (Oxford University Press, Oxford, 1999).

[12] Y. Wan and N. P. Armitage, Resolving continua of fractional excitations by spinon echo in THz 2D coherent spectroscopy, Phys. Rev. Lett. **122**, 257401 (2019).

[13] Z.-L. Li, M. Oshikawa, and Y. Wan, Photon echo from lensing of fractional excitations in Tomonaga-Luttinger spin liquid, Phys. Rev. X **11**, 031035 (2021).

[14] J. J. Lin and J. P. Bird, Recent experimental studies of electron dephasing in metal and semiconductor mesoscopic structures, J. Phys.: Condens. Matter **14**, R501 (2002).

[15] F. Evers and A. D. Mirlin, Anderson transitions, Rev. Mod. Phys. **80**, 1355 (2008).

[16] M. Woerner, W. Kuehn, P. Bowlan, K. Reimann, and T. Elsaesser, Ultrafast two-dimensional terahertz spectroscopy of elementary excitations in solids, New J. Phys. **15**, 025039 (2013).

[17] J. Lu, X. Li, Y. Zhang, H. Y. Hwang, B. K. Ofori-Okai, and K. A. Nelson, Two-dimensional spectroscopy at terahertz frequencies, Top. Curr. Chem. **376**, 6 (2018).

[18] J. W. McIver, B. Schulte, F. U. Stein, T. Matsuyama, G. Jotzu, G. Meier, and A. Cavalleri, Light-induced anomalous Hall effect in graphene, Nat. Phys. **16**, 38 (2020).

[19] E. Wang, J. D. Adelinia, M. Chavez-Cervantes, T. Matsuyama, M. Fechner, M. Buzzi, G. Meier, and A. Cavalleri, Superconducting nonlinear transport in optically driven high-temperature K_3C_{60}, Nat. Commun. **14**, 7233 (2023).

[20] S. A. Parameswaran and S. Gopalakrishnan, Asymptotically exact theory for nonlinear spectroscopy of random quantum magnets, Phys. Rev. Lett. **125**, 237601 (2020).

[21] F. Mahmood, D. Chaudhuri, S. Gopalakrishnan, R. Nandkishore, and N. P. Armitage, Observation of a marginal Fermi glass, Nat. Phys. **17**, 627 (2021).

[22] I. Paul, Nonlinear terahertz electro-optical responses in centrosymmetric electronic systems, arXiv:2101.04136.

[23] W. Niggemeier, G. von Plessen, S. Sauter, and P. Thomas, Current echoes, Phys. Rev. Lett. **71**, 770 (1993).

[24] E. L. Hahn, Spin echoes, Phys. Rev. **80**, 580 (1950).

[25] N. A. Kurnit, I. D. Abella, and S. R. Hartmann, Observation of a photon echo, Phys. Rev. Lett. **13**, 567 (1964).

[26] T. Micklitz, C. A. Müller, and A. Altland, Echo spectroscopy of Anderson localization, Phys. Rev. B **91**, 064203 (2015).

[27] K. Müller, J. Richard, V. V. Volchkov, V. Denechaud, P. Bouyer, A. Aspect, and V. Josse, Suppression and revival of weak localization through control of time-reversal symmetry, Phys. Rev. Lett. **114**, 205301 (2015).

[28] A. Kamenev, *Field Theory of Non-Equilibrium Systems*, 1st ed. (Cambridge University Press, Cambridge, 2011).

[29] B. L. Altshuler, A. G. Aronov, and D. E. Khmelnitsky, Effects of electron-electron collisions with small energy transfers on quantum localization, J. Phys. C **15**, 7367 (1982).

[30] M. Srednicki, *Quantum Field Theory*, 1st ed. (Cambridge University Press, Cambridge, 2007).

[31] Y. Asada, K. Slevin, and T. Ohtsuki, Anderson transition in two-dimensional systems with spin-orbit coupling, Phys. Rev. Lett. **89**, 256601 (2002).

[32] A. Weiße, G. Wellein, A. Alvermann, and H. Fehske, The kernel polynomial method, Rev. Mod. Phys. **78**, 275 (2006).